The Journal of the Society for Art and Science, Vol. 18, No. 1, pp. 28 – 39 (2019)

A Segmentation Algorithm for Reconstruction of Decorations on Arm Part of Mongolian Buddha Statue Based on Medial Axis

Amartuvshin Renchin-ochir[1)] **Enkhbayar Altantsetseg**[2)]
Kouichi Konno[1)]

1) Graduate School of Engineering, Iwate University, Iwate, Japan
2) School of Engineering and Applied Science, National University of Mongolia, Ulaanbaatar, Mongolia

amartuvshin@lk.cis.iwate-u.ac.jp

Abstract
Extracting the reconstructed decoration parts of a Buddha statue contributes to the analysis in archaeology and culture. A segmented decoration part with good precision is required for reconstructing the solid model of a decoration. This paper presents a novel segmentation algorithm of a point cloud for decoration points with a simple calculation based on divided rectangular surfaces. In our method, the decoration feature of the standard form according to a template is used to detect an exact decoration region. A differentiation graph indicating a variation of tangent vectors is introduced to extract the feature of a decoration region in a two-dimensional domain. A decoration region is detected according to higher correlation values with the decoration feature of the standard form. The proposed method is tested on the arm parts of a Mongolian Buddha statue and the effectiveness of our algorithm is confirmed and evaluated. The decoration points are segmented precisely, and the decoration and background parts are separated. Moreover, holes in the separated background are filled using a B-spline surface fitting technique for generating a complete surface model of the decoration parts and background.

1 Introduction

The brilliant gilt and bronze Tara's seven statues were made by Zanabazar, the world famous Mongolian artist and sculptor. The statues have been collection and maintained under the government's special legal protection of the national cultural heritage in Mongolia's largest Fine and Art museum. Two famous statues in the collection, called the White Tara and Akshohya, are shown in Figure 1 (a) and (b), respectively. Artists focus especially on the amazing decorations of the Tara statues because they contain the exquisite techniques performed by the human hand in the 17th century. They employ exclusive sculpture techniques such as bronze molding and decoration. Artists and archaeologists are eager to study the decorations of these statues. Some researchers assume that the bodies were sculptured first and the decoration was created on the bodies subsequently. Some other researchers assume that all the bodies might be molded from the same template. To verify the assumptions, the separation of decoration data from the bodies is effective for analysis. Therefore, the reconstruction of the separated decorations and body models from a digital statue is required.

Although many segmentation methods have been studied, the existing methods are inappropriate for our problem. The segmentation methods are typically intended for subpart segmentation from mesh-based CAD models that contain the surface geometry of primitive shapes such as planes, spheres, and cylinders [1]. The other methods are intended for object segmentation from environmental data such as LiDAR [2, 3].

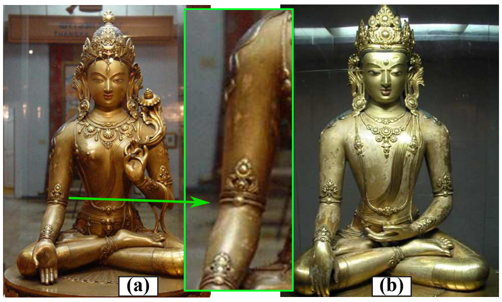

Figure 1: (a) White Tara and (b) Akshohya *(Gilt, bronze, 68x45x45). (Photographs from "http://www.zanabazarfam.mn/")*

Most segmentation algorithms for mechanical objects in reverse engineering use the model-fitting-based method with error estimation techniques [4]. For example, a descriptor-based object recognition introduced RANSAC [5]. A scanned point reconstruction method by least-squares-fitting with orthogonal distance fitting was presented [6]. The model-fitting-based methods are not suitable for our segmentation problems because the shapes of the decoration parts are handcrafted, implying their non-primitive shapes.

This paper proposes a novel segmentation algorithm that can detect small decoration parts, and is more appropriate for unorganized point clouds of Tara and other similar human-shaped statues. We herein focus, on the arm part of the statue. Convex edges around a decoration boundary are analyzed using a differentiation graph and is primary issue of our method introduced in this paper. The differentiation graph can solve the progressive mean variance of the background part, and is useful for detecting the decoration regions. According to the segmentation result, the decoration parts and the background are separated. At that time, both the hole in the background and the backside of the decoration part are filled with points, generated by the fitted B-spline surface. Therefore, the evaluation method is applied to the segmentation result for defining the accuracy of the segmentation method.

2 Related works

Several methods that have been studied could segment individual faces from a CAD object. Those methods are generally based on region-growing, explicit-boundary-based, and other combined techniques for considering the discontinuity around the sharp edges bounded by the target surface parts [7, 8].

The region-growing-based methods and their application fields are wide. The methods typically depend on the homogeneity of target regions that belong to the faces of the object surfaces. These methods are useful for surfaces comprising larger smooth regions [7, 9, 10].

The first most related method [8] could segment small patches of decorations from the primary object. It is based on the curvature of subregions with region-growing segmentation. Although the growing process is restricted owing to the sharp edges of the curvature, they concluded that their method [8] is suitable for the CAD of mechanical objects with clear mesh-based surfaces, and that it does not work for unorganized point clouds.

The second most related work [11] was applied to the segmentation of a dental model. Their method is based on a segmentation field, solved by a linear system defined by a Laplace-Beltrami operator with the Dirichlet boundary condition. A segmentation boundary is extracted on the contour lines connecting continuous concave parts that separate the teeth from the gum regions.

In summary, the decorations were created using traditional sculpture techniques that involve wrapping on the winding object surfaces of the statues. In our case, the decoration parts are narrow and branched, and the shapes are nonprimitive. Additionally, the experimental model was scanned with lower precision and overlapped surfaces around the decoration parts. Therefore, the existing methods invented for CAD models and LiDAR data are unfeasible for our segmentation problems.

3 Method overview

In this study, we applied our method to the bracelet and the chain-shaped accessories on Tara's arm, as shown in the enlarged view of Figure 1 (a). The accessories in the subarea of the target object are called *"decoration"*, and the other body surfaces are called *"background"*.

Our method consists of two primary parts. One is feature extraction using a differentiation graph and the other is decoration region extraction using decoration features of the standard form introduced in our method. The process of feature extraction is summarized in the following steps.

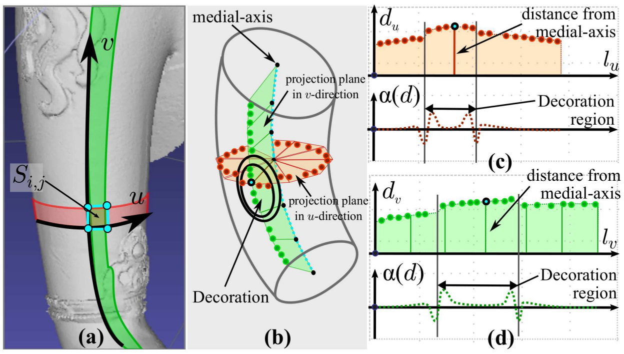

Figure 2: (a) Rectangular area $S_{i,j}$ and 'u' and 'v' directions, (b) projected inner points of two groups, (c) u-directional, and (d) v-directional points in two-dimensional domains and their differentiation graphs.

Step 1: The input point cloud is divided into a rectangular surface mesh defined by $S_{i,j}$. In the surface mesh, the direction of the cross-section is called the "u-direction" and the other direction along the trajectory is called the "v-direction", as illustrated in Figure 2 (a). The rectangular surface classification in the u- and v-directions is explained in section 3.1.

Step 2: One group of the surfaces is created in the u-direction, and the other in the v-direction, as visualized by the red and green areas in Figure 2 (a).

Step 3: The local projection planes are created for the surfaces in each of the u- and v-directions. The cross-sectional projection planes in the u-direction are visualized by red, and the projection planes in the v-direction are visualized by green in Figure 2 (b). The inner points of a target surface are projected onto each local projection plane in both the u- and v-directions. Each projected point is expanded two-dimensionally as displayed in the upper graphs of Figure 2 (c) and (d), respectively. The details of this step are explained in section 3.1.

Step 4: The differentiation graphs are defined by the expanded points of the surfaces in both the u- and v-directions. Each of the differentiation graph is illustrated in the lower graphs of Figure 2 (c) and (d). The calculation process is explained in section 3.2.

For extracting a decoration region, the following steps are to be completed.

Step 1: The decoration feature of the standard form is formulated around the boundary of the decoration using a cross-sectional shape of the decoration regions. The details are explained in section 3.3.1.

Step 2: Using features calculated by the differentiation graph, the start and end positions of the decoration regions are determined by the higher correlation value with the decoration feature of the standard form. The points in the decoration region are obtained as segmented decoration points.

Step 3: A precise segmentation area is modified and clustered. The input point cloud is separated into the decoration and background point sets.

Once the decoration points are separated, the B-spline surface fitting method is applied to the background point set to fill a hole left after the decoration points are separated. Subsequently, the backside of the decoration part is created using the completed background part.

3.1 Rectangular surface classification of input points

The main process starts from the extraction of a medial axis from an input point cloud by the L1 medial skeleton algorithm [12]. The sample points $\mathbf{c}_i$ on the medial axis is derived in the equal distance, as drawn by the green curve in Figure 3 (a). Three vectors. i.e. the tangent $\mathbf{t}_i$, normal $\mathbf{n}_i$, and bi-normal $\mathbf{b}_i$ at $\mathbf{c}_i$ are calculated by the

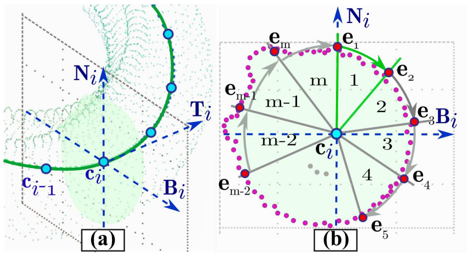

Figure 3: (a) Points $\mathbf{c}_i$ and its local coordinate system and cross-sectional plane, (b) radial-lines and their corners on the surface boundary shown by red dots.

medial axis. The direction of $\mathbf{N}_i$ is the average of the vectors obtained by the equation $\sum_{k=1}^{K} \mathbf{n}_{i-k}$, where K is the number of vectors. In this case, we set K as 5, considering variation of vector $\mathbf{n}_i$. In addition, the direction of vector $\mathbf{T}_i$ is the same as that of $\mathbf{t}_i$, $\mathbf{B}_i$ is derived from cross product of $\mathbf{N}_i$ and $\mathbf{T}_i$. Three orthogonal vectors $\mathbf{B}_i$, $\mathbf{N}_i$, and $\mathbf{T}_i$ are defined by a local coordinate system at $\mathbf{c}_i$. The cross-sectional plane is defined easily from the tangent vector $\mathbf{T}_i$ and point $\mathbf{c}_i$. The cross-sectional plane at $\mathbf{c}_i$ is divided into the same angles by m radial lines, as shown in Figure 3 (b). The purple dots are the projection of the input points near the cross-sectional plane. Points $\mathbf{e}_i$ on each of the radial lines are selected if they are closest to the input point. Each point of $\mathbf{e}_i$ should be considered at a corner of surface $S_{i,j}$.

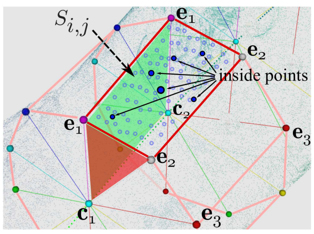

Figure 4: Surface $S_{i,j}$ and a point set involved in $S_{i,j}$.

The boundary of surface $S_{i,j}$ can be created from $\mathbf{e}_i$ and $\mathbf{e}_{i+1}$ at $\mathbf{c}_i$, and $\mathbf{e}_{i+1}$ and $\mathbf{e}_i$ at $\mathbf{c}_{i+1}$. For example, Figure 4 shows the surface bounded by $\mathbf{e}_1$, $\mathbf{e}_2$ at $\mathbf{c}_1$ and $\mathbf{e}_1$, $\mathbf{e}_2$ at $\mathbf{c}_2$. The inner points of surface $S_{i,j}$ are illustrated by blue dots in Figure 4. All surfaces $S_{i,j}$ are created similarly.

Our method creates two groups of surfaces. One is the surface in the u-direction illustrated by the red region in Figure 2 (a), and the other in the v-direction illustrated by the green region. The inner points of $S_{i,j}$ are illustrated with blue dots in Figure 5 (a). The inner points are expanded into two-dimensional information through projection.

The cross-sectional projection plane, defined from points $\mathbf{e}_i$, $\mathbf{e}_{i+1}$, and $\mathbf{c}_i$, is called the "u-plane". The other plane defined from $\mathbf{c}_i$, its points $\mathbf{e}_i$ and point $\mathbf{e}_i$ at $\mathbf{c}_{i+1}$ is called the "v-plane". If a group of surfaces is

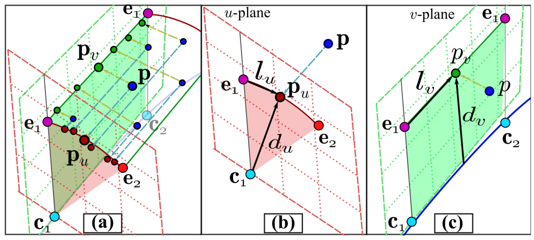

Figure 5: Definition of u- and v-planes.

created in the u-direction, the inner points are projected onto the u-plane, as shown in Figure 5 (b). The projected points are expanded to a two-dimensional domain with d_u and l_u coordinates, as illustrated in Figure 2 (c). In Figure 5 (b), d_u is the distance from $\mathbf{c}_i$ to the projected point, and l_u is the distance from $\mathbf{e}_1$ to the projected point. For the group of surfaces created in the v-direction, the inner points are projected to the v-plane as shown in Figure 5 (c). The projections of points are expanded into a two-dimensional domain, with the same information as the u-directional one.

After the projected points are expanded into the two-dimensional domains, the inner points are redefined from d and l coordinates to locate the points along the horizontal axis. Furthermore, if the group of surfaces is created in the u-direction, the expanded points are periodic on the l axis because the u-direction is derived from a cross-section. In contrast, the leftmost and rightmost expanded points are neighbors on the l axis.

3.2 Differentiation graph

The expanded points $\mathbf{p}_i$ are illustrated in the domain with l and d axes in Figure 6 (a). Generally, the start and end points of greater convexity can indicate the decoration regions, which can be assumed and highlighted by the vertical whiter bands in Figure 6 (a). Determining the method to detect the convex edges and avoiding the progressive mean-variance of the background are the problems. The differentiation graph that indicates a variation of two tangent vectors at each point $\mathbf{p}_i$, can solve this progressive mean-variance problem.

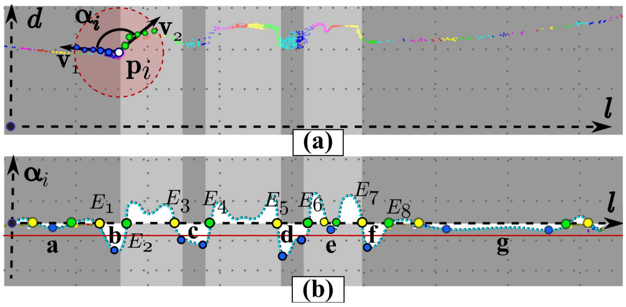

Figure 6: (a) Left and right points nearest to $\mathbf{p}_i$ and approached tangent vectors and (b) differentiation graph and its feature points.

The differentiation graph calculation is realized in the following steps.

Step 1: The points nearest to $\mathbf{p}_i$ with a user-defined radius are obtained and divided into the left and right sides as $\{\mathbf{p}_{i-a}\}$ and $\{\mathbf{p}_{i+b}\}$, respectively. a and b indicate the number of left and right nearest points, respectively, and they depend on the radius, as shown by the red circle in Figure 6 (a). In our case, we set the radius as 0.4, similar to the experimental result. If the distance is smaller, the differentiation graph could be more sensitive to variations in $\mathbf{p}_i$. Points $\{\mathbf{p}_{i-a}\}$ are shown by blue dots and $\{\mathbf{p}_{i+b}\}$ by green dots in the red circles in Figure 6 (a).

Step 2: The approached tangent vector $\mathbf{v}_1$ of points $\{\mathbf{p}_{i-a}\}$, and vector $\mathbf{v}_2$ of points $\{\mathbf{p}_{i+b}\}$ are derived using linear least square, as illustrated at points $\mathbf{p}_i$ in Figure 6 (a).

Step 3: Angle α_i of vectors $\mathbf{v}_1$ and $\mathbf{v}_2$ is solved by Eq. (1).

$$\alpha_i = arccos\left(\frac{\mathbf{v}_1 \cdot \mathbf{v}_2}{|\mathbf{v}_1||\mathbf{v}_2|}\right) \tag{1}$$

These steps are repeated for each point $\mathbf{p}_i$, after the differentiation graph is defined as shown in Figure 6 (b).

3.3 Decoration region detection

This section introduces the decoration region extraction method based on the feature of the differentiation graph.

Initially, the feature points in the differentiation graph are determined to obtain the candidate for the **start** and **end** positions at a decoration region. The feature points are the ones shown as blue, green, and yellow dots in Figure 6 (b). The blue dots are the local minimums (E_{min}), the green ones are the positive slope edges (E_{pos}), and the yellow ones are the negative slope edges (E_{neg}).

Using the feature points, the concave areas are defined as regions from "a" to "g" in the differentiation graph in Figure 6 (b). Point E_{min} is found between E_{neg} and E_{pos} in a concave area. For example, concave area "b" in Figure 6 (b) is defined from E_1 to E_2.

In Figure 6 (b), a decoration region appears from E_{pos} of a green point to E_{neg} of a yellow one. For example, E_2 is the **start** position and E_3 is the **end** position of a decoration region. However, concave areas such as "a", "e", and "g" do not always indicate the decoration regions. In our method, therefore, the value of E_{min} illustrated as a blue point is used for obtaining sufficient concave areas. If the value of E_{min} is located higher than the threshold shown by the horizontal red line, points E_{pos} and E_{neg} of the concave area can indicate the candidate of the **start** and **end** positions at a decoration region as points from E_1 to E_8. However, all candidates do not indicate the **start** and **end** positions of a decoration region such as E_1 and E_8. Point E_1 appeared only as an effect when a differentiation graph is calculated around E_2. Therefore, the candidates are determined by considering the decoration feature of the standard form defined in the following sections.

3.3.1 Decoration feature of the standard form in two-dimensional domain

Cross-sectional shapes including the decoration regions can be found around the boundary of the decoration, as illustrated by the blue line in the red circle in Figure 7 (a). If the cross-section expanded in the two-dimensional space similarly as introduced in section 3.1, the shape is represented by blue dots as shown in Figure 7 (b). The **level difference** between the background and decoration region in the vertical axis is the interesting feature to determine the decoration boundary. To reduce the calculation cost, a simple formulation of the level difference is introduced as a linear function in Figure 7 (c), according to the shape of the graph in Figure 7 (b). In the graph of Figure 7

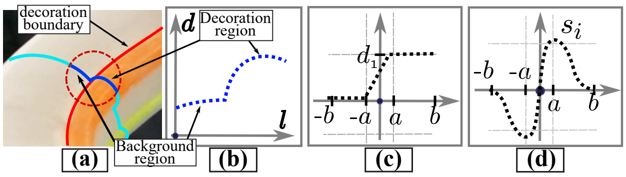

Figure 7: (a) Cross-sectional shape at the decoration boundary, (b) its expanded graph in two-dimensional domain, (c) simply formulated level difference, and (d) decoration feature of the standard form s_i.

(c), d_1 indicates the level variation difference background and decoration region of the standard form. The change between the background and decoration region is defined from $-a$ to a, the background region is defined from $-b$ to $-a$, and the decoration region is defined from a to b on the horizontal axis. Furthermore, we calculated the differentiation graph of the standard form as a black dotted line, as shown in Figure 7 (d). This graph is referred to as *the feature of the standard form*, and is used to detect an exact **start** and **end** position of a decoration region in our method.

3.3.2 Determination of start and end positions using a template of standard form

To determine the exact **start** and **end** points of the decoration region, a differentiation graph around the candidates is considered. The differentiation graph around E_4 in the red box is shown in Figure 8 (a) as an example. The differentiation graph around a candidate is re-sampled by a linear interpolation with the given $2N + 1$ number of samples. The

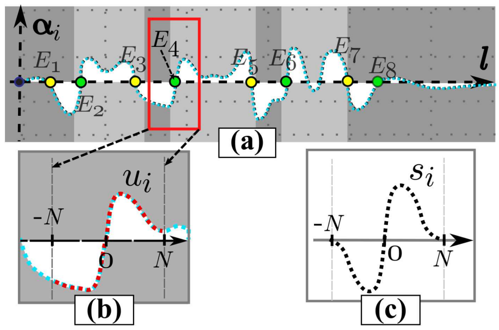

Figure 8: (a) Candidate points E_1 to E_8 in differentiation graph, (b) re-sampled differentiation graph around E_4 and (c) the re-sampled decoration feature of the standard form s_i.

re-sampled graph u_i, where $i = \{-N, ..., N\}$ of the differentiation graph around E_4, is drawn by the dotted red line in Figure 8 (b) is shown as an example. The band width of u_i is equal to $2b$, i.e., the same as the standard form. u_0 is centered at candidate E_4. The decoration feature of the standard form is resampled similarly, and defined by s_i as shown in Figure 8 (c).

If the shape of u_i is similar to s_i, candidate E_4 is selected as the **start** position of a decoration region. The degree of similarity between graph u_i and s_i is calculated by Eq. (2) for each candidate:

$$\mu_k = \frac{\sum_{i=-N}^{N} s_i u_i}{\sum_{i=-N}^{N} s_i^2} \tag{2}$$

where k is an index of candidate points E_k. The calculated degree of similarity μ_k at each candidate E_k, where $k = \{1, ..., 8\}$, is visualized by the vertical red lines in Figure 9 as an example.

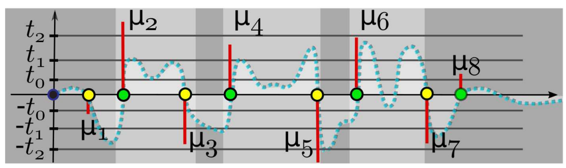

Figure 9: Calculated degree of similarity μ_k for each candidate.

If the degree of similarity μ_k is greater than the user-defined threshold, E_k indicates the **start** or **end** position of a decoration region. When a suitable threshold value is specified, a decoration region can be detected more accurately in both the u- and v-directions. Because the shape of the decoration region does not rely on each direction, the similarity μ_k is not specified in each direction. In Figure 9, three different threshold values t_0, t_1, and t_2 are illustrated as an example. When a threshold value is much lower such as t_0 in Figure 9, the inappropriate regions are extracted. In contrast, if a threshold value is much higher such as t_2, the corresponding decoration region would be eliminated. For example, all μ_k are higher than t_0, as shown in Figure 9. In this case, the decoration region detected between E_8 and E_1 is detected as an inappropriate region if a differentiation graph is defined in the u-direction. This is because the u-direction represents the cross-sectional periodic information as mentioned earlier. Therefore, a suitable threshold value is required to extract the appropriate decoration regions. For determining a suitable threshold value, the false positive and false negative error graphs are created, and presented in the next section.

3.4 Modification of precise decoration points and evaluation method of segmentation result

When the decoration regions are determined by the method introduced in the previous section, the **start** and **end** positions of a decoration region are extended to nearest point E_{min} for defining the precise decoration region. The inner points of the decoration region are obtained as segmented decoration points. In other words, decoration points that are detected in both the u- and v-directional analyses are united in one point set as the segmentation result. After the decoration parts are segmented, unexpected points may be detected as decoration points. The point density and noise of the original model are important factors to detect unexpected points. Thus, the modification process is focused on the removal of outliers in the segmentation results. The flow of the proposed modification process is shown in Figure 10.

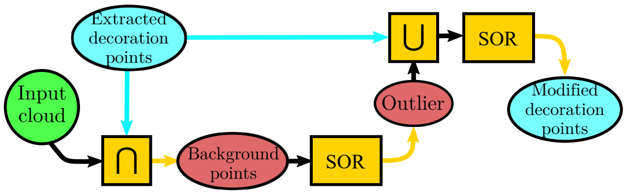

Figure 10: Flow of modification process.

A background point set is derived from the intersection of the input cloud and decoration points. The outlier points are detected by the statistical outlier removing(SOR) [13] filter from the background. Subsequently, the decoration result is modified by the SOR filter applied to the union set of outliers and extracted decoration points. The modified decoration point set is grouped into different decoration parts by the Euclidean-distance-based clustering method [14].

To determine the efficiency of our algorithm and obtain a suitable threshold value as introduced in section 3.3.2, the evaluation method is introduced and applied to the segmentation result. The ground truth of the decoration parts is separated from the input point cloud by manual operations. The number of points of the ground truth is defined by N. The undetected and over-detected points are determined using the ground truth and the segmentation result. The number of undetected points is defined by U_N. The number of over-detected points is defined by O_N.

Using U_N and O_N, the false positive errors are calculated by the equation: $FP = \frac{U_N}{N}$, and the false negative errors are calculated by $FN = \frac{O_N}{N}$. If the threshold value is high, O_N is low but U_N is high. Thus, the error ratio of the segmentation result is defined by the equation: $ER = \frac{U_N+O_N}{N}$. Our segmentation algorithm is examined with different threshold values. The error ratio ER is calculated for each segmentation result. Therefore, the suitable threshold value is determined by analyzing the error ratios.

4 Experimental results

The proposed algorithm is applied to the right arm of the White Tara model with a bracelet decoration on the upper-arm and another decoration on the shoulder. The decoration points are displayed in the areas with red boundaries in Figure 11 (a), and points $\mathbf{c}_i$ are shown by light blue dots in the enlarged views. The two different views of the inner points of the

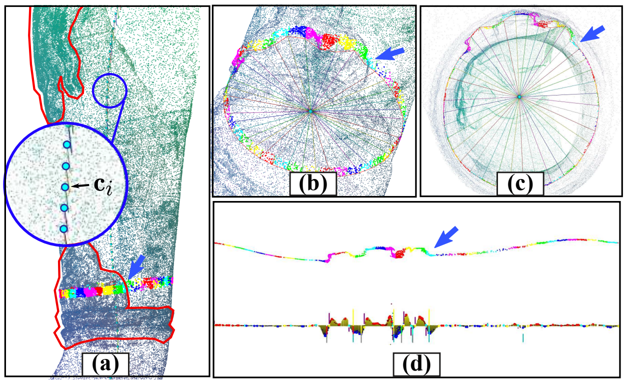

Figure 11: (a) Point cloud and its medial axis, (b) inner points of surfaces via u-direction and (c) view from other viewpoint and (d) expanded points of surfaces in 2D domain (upper graph), and its differentiation graph (lower graph).

surfaces in the u-direction are shown in Figure 11 (b) and (c), respectively. The inner points of each surface are drawn in the same color in (b) and (c). The points of the surfaces are expanded into the two-dimensional domain, as shown in the upper graph of Figure 11 (d). The blue arrows point to the same surface in all graphs of Figure 11.

The inner points of another group of surfaces in the u-direction are expanded, as shown in the upper graph in Figure 12. Points from E_1 to E_6 are the candidates for the start and end points of a decoration region in the enlarged view of the differentiation graph in Figure 12. The points E_1 and E_6 are detected as the **start** or **end** positions, and the precise decoration region is extended to the nearest point E_{min}. In Figure 12, the black vertical lines indicate the precise decoration region. The input cloud is classified into 40 surfaces in the u-direction and 71 surfaces in the v-direction, as shown in the previous examples in Figure 11 and 12, respectively.

Figure 13 shows the segmentation result in the u- and v-directions. The points detected in both the u and v-directions are shown by green

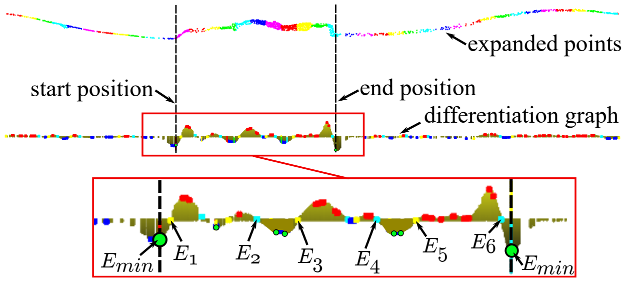

Figure 12: Expanded points of other surfaces (upper graph), its differentiation graph (lower graph) and the enlarged view of the differentiation graph in the red rectangle.

dots. The result of the segmentation in the u-direction is shown by purple dots and that in the v-direction is shown by blue dots in Figure 13.

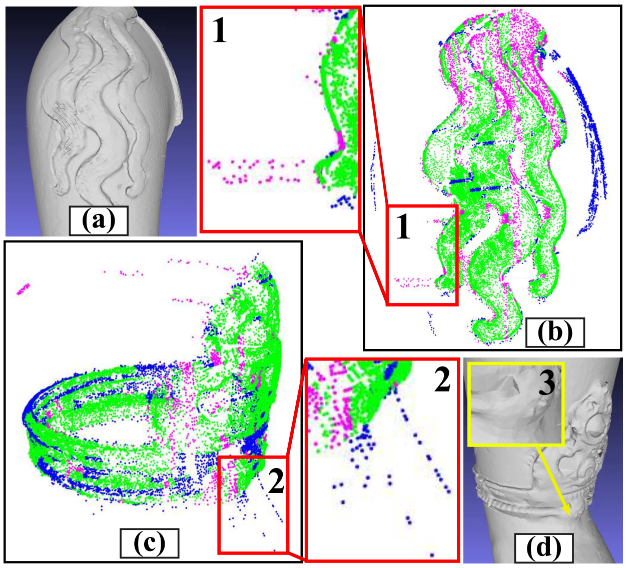

Figure 13: (a) Decoration on the shoulder, (b) its segmented points, (c) segmentation result of bracelet decoration, and (d) its solid model.

The outliers detected in the u-direction are shown in the enlarged view 1 in Figure 13 (b) by purple dots. The ones detected in the v-direction are shown in the enlarged view 2 in Figure 13 (c) by blue dots. However, the outliers can be removed by the SOR filter because the distribution of the outliers is narrow.

The final result of our examination is shown in Figure 14 (a). The clustered decoration parts are classified into point sets of different colors.

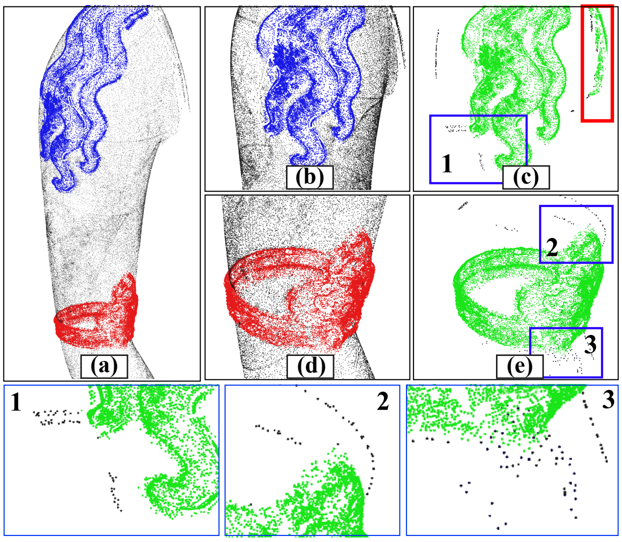

Figure 14: (a) Segmentation result, (b) decoration on the shoulder (c) point cloud before modification, (d) segmented decoration of bracelet (e) point cloud before modification. *(Black points are the outliers removed by SOR in enlarged views from 1 to 3.)*

The black points indicate the background (arm surface), the blue points indicate the decoration part on the shoulder, and the red points indicate the bracelet decoration part. In the images (c), (e), and enlarged views 1, 2, and 3 in Figure 14, the green points indicate that the modified decoration points and black points are outliers. The points in the red rectangle are the decoration part left from the Tara's chest, as shown in the original arm model in Figure 13 (a). Even if those points are detected and clustered as a decoration part, it is a part of the shoulder. Therefore, it is removed by manual operation.

The separated background set around the holes are as shown in Figure 15 (a) and (c). The points that fill the holes are generated by a fitted B-spline surface illustrated by the orange points in Figure 15 (b) and (c).

4.1 Evaluation results

The segmentation result is illustrated by black and blue points in Figure 16 (a) when the threshold value is 0.3. The separated point set of the ground truth is illustrated by the green

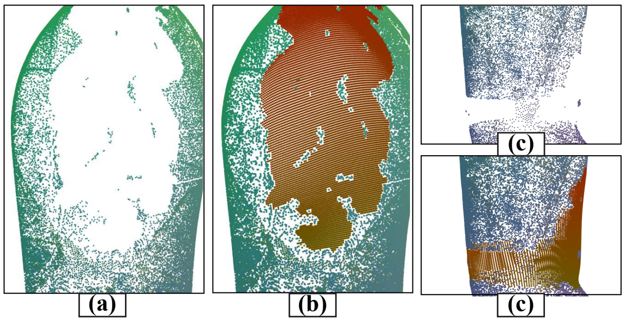

Figure 15: (a) (c) Holes on the separated background cloud, and (b) (d) filling results of the holes.

points in Figure 16 (b). The number of points is defined by N. The undetected points defined by U_N are illustrated by red points in Figure 16 (c). The over-detected points defined by O_N are illustrated by the black dots in Figure 16 (a).

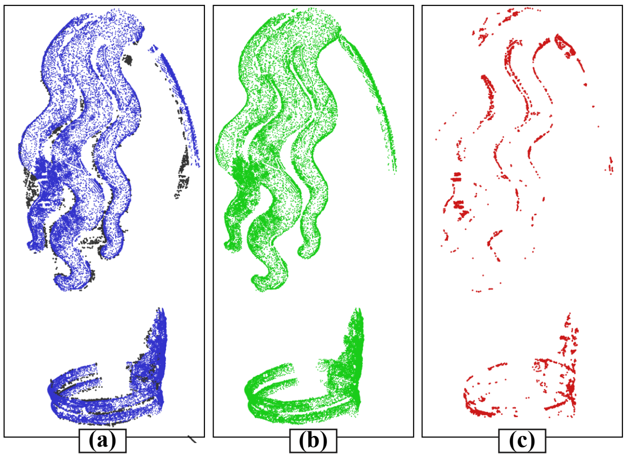

Figure 16: (a) Segmentation result with over-detected points, (b) ground truth points, and (c) undetected points.

The false positive graph is defined as FP and the false negative graph is defined as FN, as plotted in Figure 17. In these graphs, the horizontal axis indicates the threshold value, and the vertical axis indicates an FP in the top side and an FN in the bottom side.

The segmentation results with over-detected points are illustrated in Figure 18 when the threshold values are 0.1, 0.2, and 0.5. The error ratio of the segmentation result is defined by $ER = \frac{U_N + O_N}{N}$ and plotted by the orange points in Figure 17.

The analysis of the graphs indicate that the

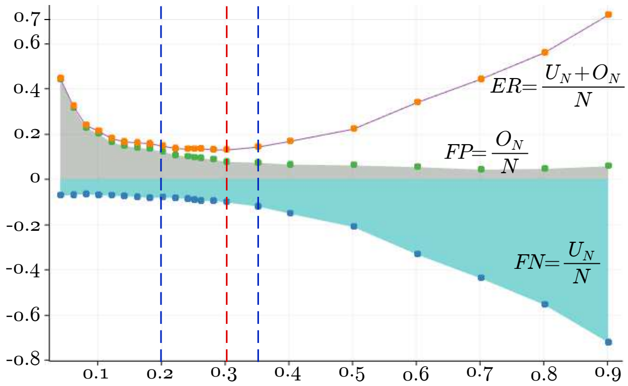

Figure 17: False positive and false negative error graphs, and error ratio graph of the segmentation result.

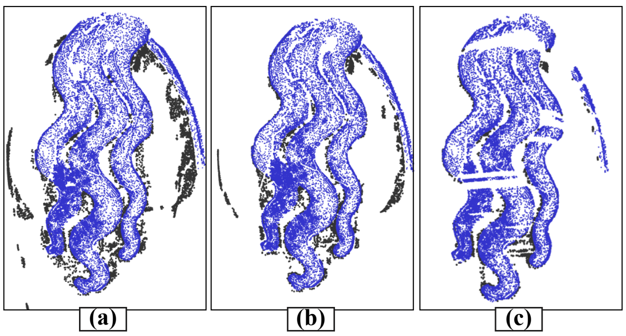

Figure 18: (a) Segmentation result when the threshold value is equal to 0.1, (b) 0.2 and (c) 0.5.

minimum error ratio is 0.128 when the threshold value is 0.3. According to this analysis, 0.3 is chosen as the suitable threshold value to determine the exact **start** and **end** positions of the decoration region in both the u- and v-directions. However, when the threshold value is in the range of 0.2 to 0.35, the error ratio is smaller than 0.15. Therefore, the threshold value can be chosen in this range, considering the sufficient number of decoration and background points for creating the solid models of the decoration parts.

The proposed method is implemented using the C++ programming language and an open-source visualization toolkit library (VTK), with an Intel Core i7-6700 CPU and 8GB RAM. The total processing time of the segmentation is approximately 137 seconds on the unorganized cloud with 90k points. The decoration parts are clustered as shown in Figure 14 (a) and the accuracy of the segmentation method was 87.2% which is well enough for the next study to make solid models of arm model, assuming the evaluation result.

In this experiment, the method [12] extracts one skeleton branch from the input cloud because our algorithm functions for one ground in the medial axis. Therefore, the decoration parts were contiguous on the surface. Furthermore, the shape of the arm model is cylindrical in the u-direction and bent smoothly in the v-direction. Analyzing those characteristics of the model, the algorithm is suitable for application to the smoothly curved model with one medial axis. The number of medial axis is considered as a limitation of our algorithm.

5 Conclusion and Future Works

A novel algorithm was proposed and implemented for decoration point segmentation. The algorithm was tested on the white Tara's right-arm model comprising two decoration parts on the shoulder and upper-arm. The segmentation was intended to separate the organized decoration points from unorganized point clouds with good precision. However, it depended comparatively depends on the density of point clouds in the analysis in two-directions, which could be modified. The hole on the separated arm part was filled using a B-spline surface approximation based on the segmentation result as presented in Figure 15. The basic concept of our method had already been presented in NICOGRAPH 2017 [15], and we extended the concept in this paper.

In our future work, we will create solid models of the decoration parts, using points generated in the background holes. In addition, we will test our method on other parts of the statues that consist of two or more skeleton branches, to increase the possibility of the segmentation algorithm.

Acknowledgment

This research is partially supported by MJEED JR14B16 project and bilateral programs in JSPS.

Furthermore, we are extremely grateful for lots of efficient advice received from the paper reviewers.

References

[1] A.Agathos, et al., 3D mesh segmentation methodologies for CAD applications. Computer-Aided Design and Applications, Vol: 4, No.6, pp.827-841, 2007.
[2] B. Douillard, et al., On the segmentation of 3D LIDAR point clouds. In Robotics and Automation (ICRA), 2011 IEEE International Conference on. pp. 2798-2805, 2011.
[3] T. Hackel, J.D. Wegner and K. Schindler, Fast Semantic Segmentation of 3D Point Clouds with Strongly Varying Density, In: ISPRS Ann. Photogramm. Remote Sens. Spatial Inf. Sci., Vol. 3, No.3, pp. 177-184, 2016.
[4] E. Grilli, F. Menna and F. Remondino, A Review of Point Clouds Segmentation and Classification Algorithms. ISPRS-International Archives of the Photogrammetry, Remote Sens. Spatial Inf. Sci., pp.339-344, 2017.
[5] C. Papazov and D. Burschka, An Efficient RANSAC for 3D Object Recognition in Noisy and Occluded Scenes, In: ACCV 2010, LNCS 6492, pp. 135-148. Springer, 2011
[6] S.J. Ahn, Least Squares Orthogonal Distance Fitting of Curves and Surfaces in Space, In: LNCS 3151, Springer, 2004.
[7] Anh-Vu. Vo, et al., Octree-based Region Growing for Point Cloud Segmentation. ISPRS J. Photogramm. Remote Sens., vol. 104, pp. 88-100, 2015.
[8] G. Lavoué, F. Dupont and A. Baskurt, A New CAD Mesh Segmentation Method, Based on Curvature Tensor Analysis, In: CAD, Vol. 37, No. 10, pp. 975-987, 2005.
[9] J.-E. Deschaud and F. Goulette, A fast and Accurate Plane Detection Algorithm for Large Noisy Point Clouds using Filtered Normals and Voxel Growing, Proc. of 3DPVT Conf., 2010.
[10] A. Nurunnabi, D. Belton and G. West, Robust Segmentation in Laser Scanning 3D Point Cloud Data. 2012 In: Int. Conf. on DICTA, IEEE, pp. 1-8, 2012.
[11] Z. Li and H. Wang, Interactive Tooth Separation from Dental Model Using Segmentation Field, In PloS one, Vol. 11, No. 8, DOI:10.1371, 2016.
[12] H. Huang, et al., L1-Medial Skeleton of Point Cloud, In: ACM Trans. on Graph., vol. 32, No. 4, pp. 1-8, 2013.
[13] R.B. Rusu, et al., Towards 3D Point Cloud Based Object Maps for Household Environments, In Robotics and Autonomous Syst. Journal. Vol. 56, No. 11, pp.927-941, 2008.
[14] R.B. Rusu, Semantic 3D Object Maps for Everyday Manipulation in Human Living Environments. PhD thesis, Computer Science department, Technische Universitaet Muenchen, Germany, October 2009.
[15] Amartuvshin Renchin-ochir, Katsutsugu Matsuyama, Enkhbayar Altantsetseg and Kouichi Konno, A Segmentation Algorithm for Decoration on Arm part of Mongolian Buddha Statue Based on Medial Axis, In: Proceeding of NICOGRAPH 2017, 2017.

Amartuvshin Renchin-Ochir

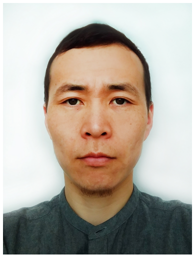

Amartuvshin Renchin-Ochir is a Ph.D. candidate of Graduate School of Engineering at Iwate University. He received the B.Sc. and M.E. degrees from the National University of Mongolia in 2007 and 2010. He worked on a lecturer of School of Engineering and Applied Sciences at National University of Mongolia from 2012 to 2016. His research interests include geometric modeling, computer vision, robotics, and computer graphics.

Enkhbayar Altantsetseg

Enkhbayar Altantsetseg received the B.S. and M.S. in mathematics from National University of Mongolia in 1995 and 1997, respectively. He earned his Dr. Eng. in design and media technology from Iwate University in 2013. He is currently a professor of School of Engineering and Applied Sciences of National University of Mongolia. His research interests include geometric modeling, virtual reality, augmented reality, and simulation.

Kouichi Konno

Kouichi Konno is a professor of Faculty of Engineering at Iwate University. He received a BS in Information Science in 1985 from the University of Tsukuba. He earned his Dr.Eng. in precision machinery engineering from the University of Tokyo in 1996. He joined the solid modeling project at RICOH from 1985 to 1999, and the XVL project at Lattice Technology in 2000. He worked on an associate professor of Faculty of Engineering at Iwate University from 2001 to 2009. His research interests include virtual reality, geometric modeling, 3D measurement systems, and computer graphics. He is a member of EuroGraphics.